Presented at the 31st European PV Solar Energy Conference and Exhibition, 14-18 September 2015, Hamburg, Germany

INVESTIGATING THE IMPACT OF PARAMETER AND PROCESS VARIATIONS ON MULTICRYSTALLINE SILICON PERC CELL EFFICIENCY

Sven Wasmer, Johannes Greulich, Hannes Höffler, Jonas Haunschild, Matthias Demant, Stefan Rein
Fraunhofer Institute for Solar Energy Systems
Heidenhofstr. 2, D-79110 Freiburg, Germany. Phone: +49 761 4588 5012.
E-Mail: sven.wasmer@ise.fraunhofer.de

ABSTRACT: In this work, we thoroughly investigate the impact of parameter and process variations in an industrially feasible multicrystalline silicon (mc-Si) passivated emitter and rear cell (PERC) process. In an experiment, where in total more than 800 mc-Si PERC cells are fabricated, we distribute 51 neighboring high-performance mc-Si wafers and characterize them in depth to garner only the process-induced variations within a larger experiment. We use numerical three-dimensional (3-D) device simulations to model the width of the resulting distribution of solar cell efficiencies of this group. The main responsible parameters leading to a broadening of the distribution are extracted and ranked by their impact, highlighting the parameters that need to be tuned and controlled most accurate. In our case, from the variations in cell efficiencies amounting to 0.9 $\%_{abs.}$, we identify the rear side passivation and a wrap-around during the emitter etch back process to be in charge of almost 60 % of the total fluctuations. With the presented approach and its findings, a better understanding of the underlying dependencies can be developed and subsequently applied to improve the ramp-up and the development of mc PERC cell production. In addition, the relevant parameters and their range obtained and denoted in this work are a fundamental input for modelling a mc-Si PERC solar cell, drawing a realistic illustration of parameters achieved in today's research facilities and during ramp-up of PERC production.
Keywords: Characterisation, Multicrystalline Silicon, PERC, Simulation

1 INTRODUCTION

With the increasing share of the so-called "high-performance" (HP) multicrystalline (mc) silicon wafers, high-efficiency solar cell concepts such as the "Passivated Emitter and Rear Cell" (PERC, [1]), which were formerly mainly limited by bulk lifetime, are getting more and more important on p-type mc-Si substrates. Combining the low-cost wafer with the PERC process seems appealing, but yet there are still issues to solve regarding process stability and quality, in particular during ramp-up of new production lines. Methods of process control for the, compared to the conventional concepts, more demanding high efficiency solar cell concepts with a passivated rear side need still to be worked out. Prior to developing these methods, the crucial parameters and processes have to be identified. Yet in order to develop a better understanding of a mc PERC process it is advisable not only to evaluate the influences on absolute solar cell efficiency (e.g. via a loss analysis [2]), but also to detect the origins of variations thereof.

In this work, we therefore summarize an approach to identify and rank the impact of the most important parameters and processes on the achieved distribution of cell efficiencies by means of 3-D numerical device simulations, similarly conducted in [3], but additionally using experimental data of manufacturing of an industrial feasible mc PERC process for determining, adjusting and fitting the input parameters of the simulations and for a comparison of the measured and simulated cell efficiencies. Within this work, we focus on the process-induced, not on the material-induced variations of the final cell efficiency.

The present work begins in section 2 with the description of our approach consisting of the experiment, where the production and characterization of the solar cells is presented (sec. 2.1), the optical and electrical simulations, where the width of the achieved efficiency distribution is modeled (sec. 2.2 and 2.3) and finally our procedure to investigate the impact of each input parameter of the simulations is summarized (sec. 2.4). We visualize the results in section 3 and discuss them in section 4. A summary and the drawn conclusions are given in section 5.

2 APPROACH

This section on the description of our approach can be divided into three parts:

Firstly, the underlying experiment is described regarding the manufactured solar cells, used measurement techniques and processing of specific samples besides the cells.

Secondly, we use Sentaurus Device [4] to conduct numerical 3-D device simulations with the goal of reproducing the width of the achieved distribution of cell efficiencies. Benefits of the simulations are the possibility of synthetically turning on and off variations of selected input parameters (e.g. base doping concentration or minority carrier bulk lifetime, see table I, or estimating magnitudes like the rear side passivation quality that are yet not directly experimentally quantifiable during the process or on cell level). Furthermore, by applying simulations instead of performing the analysis on the experimental stage alone, we are not prone to outliers and noise which are inevitable in production.

In the last part of our approach, we analyze the impact of each input parameter in a Pareto analysis, ranking the parameters according to their influence on the total variation in cell efficiency. We therefore define the variation of a parameter as the range between the 10th and the 90th percentile of this parameter, including 80 % of the data points and omitting extreme outliers. These two values, together with the median, are used as the input parameters of the simulations, later referred to as "low", "medium" and "high".

2.1 Experimental

The basis of the experiment consists of processing approximately 800 mc p-type wafers to PERC solar cells in the industrial-like environment of the Photovoltaic Technology Evaluation Center PV-TEC at Fraunhofer ISE in Freiburg [5], using the process route depicted in Figure 1 for wafers with a broad variation of material quality. In order to track only the process-induced variations and to exclude material-induced variations of the cell efficiency, we distribute 51 neighboring high-performance mc-Si wafers evenly among the other wafers. After acidic texturing, the phosphorus emitter diffusion is carried out using the process developed in ref. [6]. Afterwards, the phosphorus silicate glass (PSG) and the emitter on the rear side are removed wet-chemically. The rear side is passivated by a stack of PECVD aluminum oxide and silicon nitride and the front side by silicon nitride solely. Contacts are applied via screen printing and the front contact is formed with a firing step in a fast firing oven. For the back contact formation we use the laser fired contacts (LFC) process [7]. After a forming gas annealing step, the current-voltage characteristics of the cells are measured inline using a h.a.l.m. flasher on a Manz solar cell tester.

Furthermore, specific samples to measure the emitter dark saturation current density j_{0e} and the implied open-circuit voltage iV_{oc} are processed one per batch. For the iV_{oc}-samples, we choose every 5th wafer of the 51 neighboring wafers, extract them prior to metallization and subject them to a firing step in a fast firing oven in order to activate the passivation. To measure the bulk lifetime τ_{bulk}, symmetric lifetime samples passivated with Al_2O_3 deposited by fast atomic layer deposition are processed parallel to the solar cells up to the emitter formation on 3 wafers of the reference material.

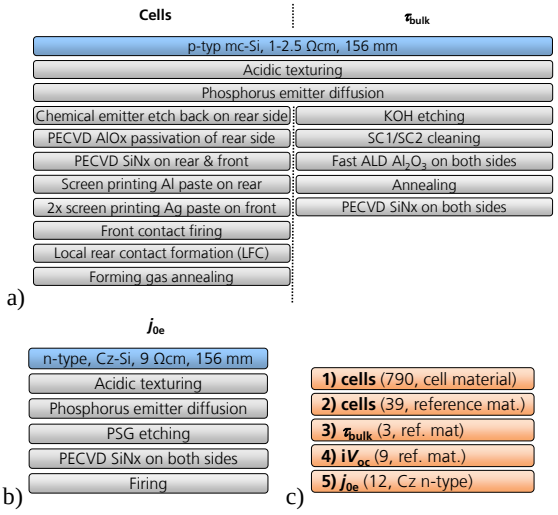

Figure 1: a) As process route, a PERC process on multi-crystalline p-type wafers is chosen as shown in the left part of the sketch. After a forming gas annealing step, the cells are measured on a h.a.l.m. flasher within a Manz solar cell tester. During each process step, several in-line and off-line measurement techniques available at PV-TEC are applied. Furthermore, in the right part of a) the process sequences of the τ_{bulk} and b) j_{0e} samples are shown. In c) an overview of the processed wafers and their quantities is given.

The process sequences for the j_{0e} and τ_{bulk} samples are given in Figure 1. After each process step of the cell process we make use of the manifold in-line and off-line measurement techniques available at PV-TEC.

The in-line methods, which are applied to every wafer, include measurements of the wafer thickness d_{Si} via capacitance, the base resistance and accordingly the doping concentration N_{dop} via induction, the reflectance after texturing at a wavelength of 600 nm R_{600nm} using a spectrometer, the thickness of the anti-reflection coating (ARC) layer d_{ARC} with an OSIS Coating tool by Optection and the emitter sheet resistance R_{sh} by comparing the resistance measurements after texturing and the emitter etch back process. At cell level, we measure the grid resistance of fingers and busbars R_{grid}, the parallel and series resistances R_p and R_s, the dark saturation current densities j_{01} and j_{02} of the two-diode model via fitting of the Suns-V_{oc} pseudo *IV* curve and finally the performance characteristics short-circuit current density j_{sc}, open-circuit voltage V_{oc}, fill factor *FF* and conversion efficiency η. In case of the wafer thickness, resistance and reflectance and the ARC layer thickness, data are obtained in a spatially resolved manner. If not otherwise stated, we use the mean value to characterize one wafer.

The off-line methods, which are only utilized for the cells of the reference material that is considered in this work, comprise spectrally resolved measurements of the reflectance, photoluminescence (PL) imaging and measurements of the specific contact resistance. The reflectance curves of the finished cells, which contain both the passivated front and the metallized part of the cell, can be used to calculate the optical finger widths w_{finger}, and consequently the shading fraction M_{met} due to the front metallization, by repeated subtraction of the reflectance spectrum of a silver finger until the expected minimum of reflectance of the unmetallized part alone is reached. The specific contact resistance is determined on spot samples via measurements conducting the transfer length method (TLM, [8]). In order to obtain the influence of the recombination at the local rear side contacts to the open-circuit voltage V_{oc} of the finished cell, we acquire PL images before and after laser contact firing. Since the intensity value $I_{PL}^{(x,y)}$, given in counts per second, at each pixel *(x,y)* of the PL image is proportional to the exponential of the local junction voltage [9] at this pixel, two images can be used to calculate an absolute voltage loss ΔV_{LFC} with the equation

$$\Delta V_{LFC} = V_T \cdot \left(\langle \ln\left(I_{PL,2}^{(x,y)}\right) \rangle - \langle \ln\left(I_{PL,1}^{(x,y)}\right) \rangle \right) \qquad (1)$$

where V_T denotes the temperature voltage which is multiplied with the difference of the mean values, depicted with the angle brackets, of the logarithmical taken PL images intensities $I_{PL}^{(x,y)}$ in both states 1 and 2, i.e. before and after LFC processing.

Concerning the specific samples for determining the implied open-circuit voltage iV_{oc} and the bulk lifetime τ_{bulk} we use quasi-steady-state photoconductance (QSSPC, [10]) lifetime calibrated PL images [11]. The iV_{oc} is determined by converting the lifetime image to local voltages and taking the mean of the resulting image. For the τ_{bulk} samples we acquire two images at 0.04 and 1 suns (considering 1 sun being equivalent to a photon flux of $2.55*10^{17}$ $cm^{-2}s^{-1}$ for the excitation wavelength of 790 nm) and calculate the harmonic mean in the diffusion length for the two lifetime images under differing injection conditions as in [12]. The emitter dark

saturation current density j_{0e} is determined with the j_{0e} samples using the Kane-Swanson method [13].

2.2 Optical simulations

For the optical simulations we use the Monte-Carlo ray tracer of Sentaurus Device and assume a temperature of the device of 25°C. For the front side consisting of a thin SiN_x layer on an iso-textured surface we utilize the transfer-matrix-formalism, whereas the rear side is modeled by the Phong model [14]. For the bulk, we assume Lambert-Beer's law, neglecting free-carrier absorption. Concerning refractive indices, we employ the values of [15] for silicon and measured values of the applied PECVD SiN_x on planar surface.

The characteristic angle $\omega_{texture}$ of the iso-texture [16] is determined by fitting the reflectance at 600 nm to the measurement after the texturing process as done in [17]. The validity of the simulated spectral reflectance in the wavelength range from 300 to 900 nm is ensured by a comparison with measured spectra of wafers after ARC layer deposition. The parameters R_0 and ω_{Phong} of the Phong model are adjusted such that the reflectance in the wavelength range between 900 and 1200 nm fits the measurement on finished cells. Since these measured reflectance spectra didn't vary to a great extent we choose one pair of values for R_0 and ω_{Phong}.

Results of the optical simulations are spectrally and spatially resolved generation profiles. For a first estimation of the impact of the input parameters in the optical simulations (see Figure 3), the depth- and wavelength- integrated photo-generated current density j_{ph} is regarded. We later consider the shading due to the front metallization M_{met} by scaling j_{ph} with $(1\text{-}M_{met})$.

Results will be given in the results section – here only the procedure and the setup is described.

2.3 Electrical simulations

We conduct the electrical simulations at a device temperature of 25°C. The depth-dependent generation profile resulting from the optical simulation is taken as input for the 3-dimensional cuboidal symmetry element with quadratic base. The base lengths are assigned half the distance between the LFC contacts, in our case 175 µm and the height corresponds to the wafer thickness. In one corner of the base a quadratic region with side length of $w_{rec,rear}$ is defined, comprising the area of damaged area by the rear contact formation process. As usual for this kind of cells (see e.g. Ref. [18]), we assume an effective front side, i.e. homogeneous resistance and recombination properties.

For the general models considering the simulation of silicon solar cells, we use the ones summarized in [19]. We follow the recommendation of Altermatt [20] to use the precisely known values of the bandgap E_g, the intrinsic charge carrier concentration n_i and the effective density of states in the conduction band N_c to adjust the least precisely known value of the effective density of states in the valence band N_v for self-consistency.

For determining the surface recombination velocity $S_{pass,front}$ of holes at the front surface of the emitter, we use the ECV profile [6], simulate injection-dependent lifetime (QSSPC) curves by varying $S_{pass,front}$ and compare the measured j_{0e} with the value fitted to the simulated curves.

Concerning the consideration of the bulk lifetime τ_{bulk} in the simulations, we fit a mid-bandgap Shockley-Read-Hall (SRH) defect to each pair of lifetime measurements at two injection levels by adjusting and averaging the parameters τ_{n0} and τ_{p0} of the 3 τ_{bulk} samples.

We estimate the surface recombination velocity $S_{pass,rear}$ of electrons at the rear side passivation by using the bulk lifetime determined in the last section and adjust the values in the cell simulation (by setting $w_{rec,rear}$ to zero) to fit the measured iV_{oc}, assuming an injection independent $S_{pass,rear}$.

For the surface recombination velocity $S_{met,rear}$ at the local rear contacts, the parametrization formerly introduced in [21] and used in [22] is applied, while the side lengths $w_{cont,rear}$ of the contacting area of a LFC contact are assumed to be half the size of that of the damaged area ($w_{rec,rear}$ = 2*$w_{cont,rear}$). We determine the size of the damaged area by varying $w_{rec,rear}$ in the simulations and comparing the resulting V_{oc} with the value when $w_{rec,rear}$ = 0 µm is assumed. The latter value corresponds to iV_{oc} since we do not consider increased recombination beneath the front contacts after contact formation. The resulting differences in V_{oc} are adjusted to fit the measured voltage losses ΔV_{LFC}.

The simulated *IV*-curves of Sentaurus Device are given in discrete tuples (V_i, j_i). In order to include non-ideal recombination (for example contributions from the bulk which are not included in our simplified model for the bulk lifetime (e.g. coupled defect level recombination [23]) and recombination at the wafer edges or in the space charge region) in our model, we add an external diode with an ideality factor of 2 and a saturation current density $j_{02,external}$ to our model, which reduces the current output at a fixed voltage:

$$j_i^{new} = j_i - j_{02}\left(\exp\left(\frac{V_i}{2V_T}\right) - 1\right) \qquad (2)$$

Furthermore, to account for the contribution of the front to the total series resistance R_s we add an external series resistance $R_{s,external}$ to the simulated *IV*-curves and consider it by reducing the voltages V_i:

$$V_i^{new} = V_i - j_i^{new} R_{s,external} \qquad (3)$$

The external series resistance comprises the contributions of the emitter sheet resistance R_{sh}, the specific contact resistance ρ_c and the resistance of the metal grid R_{grid} to the effective series resistance. Since their variations are small, we consider them in one triple of values for $R_{s,external}$, while R_{grid} being the dominant source of variation.

The integration of $j_{02,external}$ and $R_{s,external}$ is schematically depicted in Figure 2.

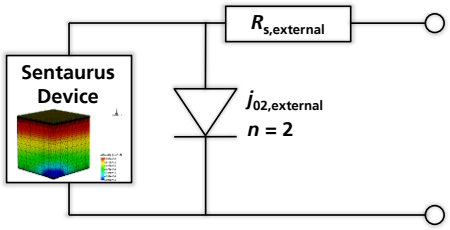

Figure 2: Schematic sketch of the integration of the diode with ideality factor 2 and the external series resistance.

Since the measured $j_{02,measured}$ obtained by fitting the two-diode model to the Suns-V_{oc} curve contain the global information of the cell, we cannot simply use these values for $j_{02,external}$. We therefore fit the two-diode model

to an exemplary (where all input parameters are kept at their median values) Sentaurus Device *IV*-curve (with $j_{02,external}$ and $R_{s,external}$ set to zero) and subtract the determined $j_{02,Sent.Device}$ from the measured ones in order to obtain meaningful values for $j_{02,external}$:

$$j_{02,external} = j_{02,measured} - j_{02,Sent.Device} \quad (4)$$

2.4 Evaluating the impact of each parameter

Each of the 6 input parameters $\omega_{texture}$, $S_{pass,rear}$, M_{met}, $w_{rec,rear}$, $j_{02,external}$ and $R_{s,external}$ (see also table I) was varied with their aforementioned three values low, med. and high in a full factorial design of experiment, resulting in 3^6 = 729 simulations. These reduce to practicable 81 Sentaurus Device processes by the subsequent possibility of consideration of $R_{s,external}$ and $j_{02,external}$.

For each of the input parameters and for each of the simulated cell performance characteristics j_{sc}, V_{oc}, *FF* and η we perform the following analysis:

1. Determine the absolute variation *var*(all) of the cell characteristic by taking the difference of the maximal and minimal value while all input parameters are varied.
2. Holding one input parameter *p* at its median value while varying all others and again calculating the difference of the resulting max. and min. values of the characteristic *var*(w/o *p*).
3. Subtracting the variation when one input parameter is not varied from the variation when all are varied: *var*(*p*) = *var*(all) - *var*(w/o *p*).

This so defined value *var*(*p*) corresponds to the derogation of the distribution of the target solar cell performance characteristic if the input parameter *p* would have no fluctuations and is therefore a measure of its impact on the broadening of the resulting distribution. If interactions of p_i with each other are absent, all impacts *var*(p_i) should sum up to the total variation *var*(all):

$$\sum_i var(p_i) \cong var(\text{all}) \quad (5)$$

In the results and in the discussion section we show that this is the case here.

3 RESULTS

The input parameters to the simulations are given in table I along with their low, medium and high values determined from the experiment. We neglect variations in the wafer thickness d_{Si} and the ARC layer thickness d_{ARC} since they introduce only a minor variation in the present optical simulations of j_{ph} compared to the characterstic angle of the iso-texture, as can be seen in Figure 3.

The fit of the mid-bandgap SRH defect results in values of τ_{n0} = 24 µs and τ_{p0} = 910 µs.

The experimentally achieved and simulated distributions of the short-circuit current density j_{sc}, the open-circuit voltage V_{oc}, the fill factor *FF* and the efficiency η are depicted in Figure 4 as histograms. Note that our approach is aimed at reproducing the width of the resulting distribution and therefore the shape is not reflected accurately.

The results of the approach introduced in section 2.4 regarding the impact of each input parameter on the total variation the cell characteristics j_{sc}, V_{oc}, FF,and η in the simulations is given in Figure 5 as Pareto diagrams, ranked by their impact on variation in cell efficiency.

Table I: Input parameters to the simulations. Variations of parameters labeled with (*) are not considered in the electrical simulations because of their vanishing influence.

	Low	Med.	High
d_{Si} (µm) (*)	183.7	185.4	186.2
N_{dop} (cm^{-3})	-	$9*10^{15}$	-
τ_{n0} (µs)	-	24	-
τ_{p0} (µs)	-	910	-
$\omega_{texture}$ (°)	56.5	57.8	61.0
j_{0e} (fA/cm^2) | $S_{pass,front}$ (cm/s)	-	92 | $2.5*10^5$	-
d_{ARC} (nm) (*)	77.5	79.6	82.2
R_0 (Phong model)	-	0.935	-
ω (Phong model)	-	2	-
$S_{pass,rear}$ (cm/s)	70	130	300
$S_{met,front}$ (cm/s)	-	$S_{pass,front}$	-
M_{met} (%)	3.98	4.31	4.58
$w_{rec,rear}$ or $2*w_{cont,rear}$ (µm)	32.5	39	45
$j_{02,external}$ (nA/cm^2)	5.5	12	23.5
$R_{s,external}$ (Ωcm^2)	0.523	0.547	0.596

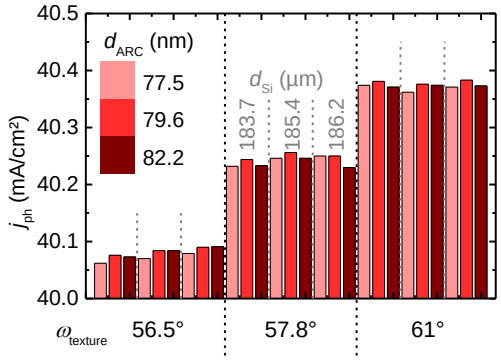

Figure 3: Results for the photo-generated current density j_{ph} where the wafer thickness d_{Si}, the ARC layer thickness d_{ARC} and the characteristic texture angle $\omega_{texture}$ are varied in the optical simulations. Most impact (~ 0.3 mA/cm^2) appears to be caused by $\omega_{texture}$ and we therefore neglect the other two parameters in the subsequent discussion.

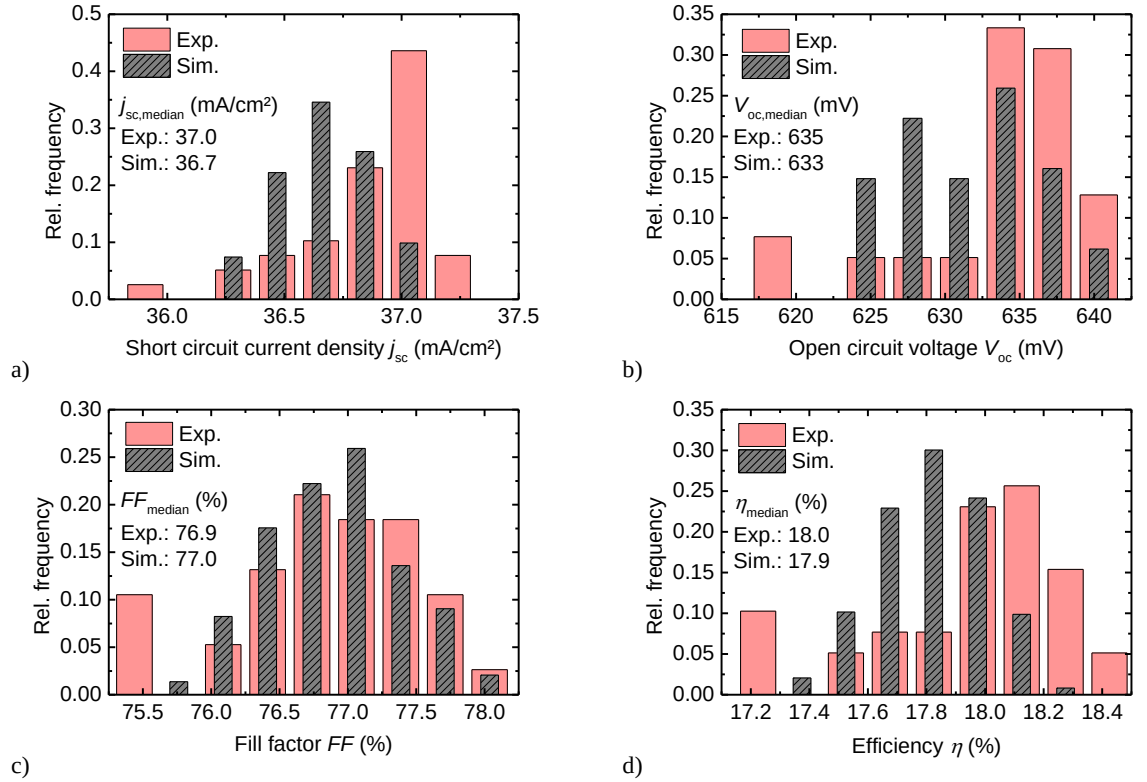

Figure 4: Experimentally achieved and simulated distributions of the four cell characteristics a) j_{sc}, b) V_{oc}, c) FF and d) η.

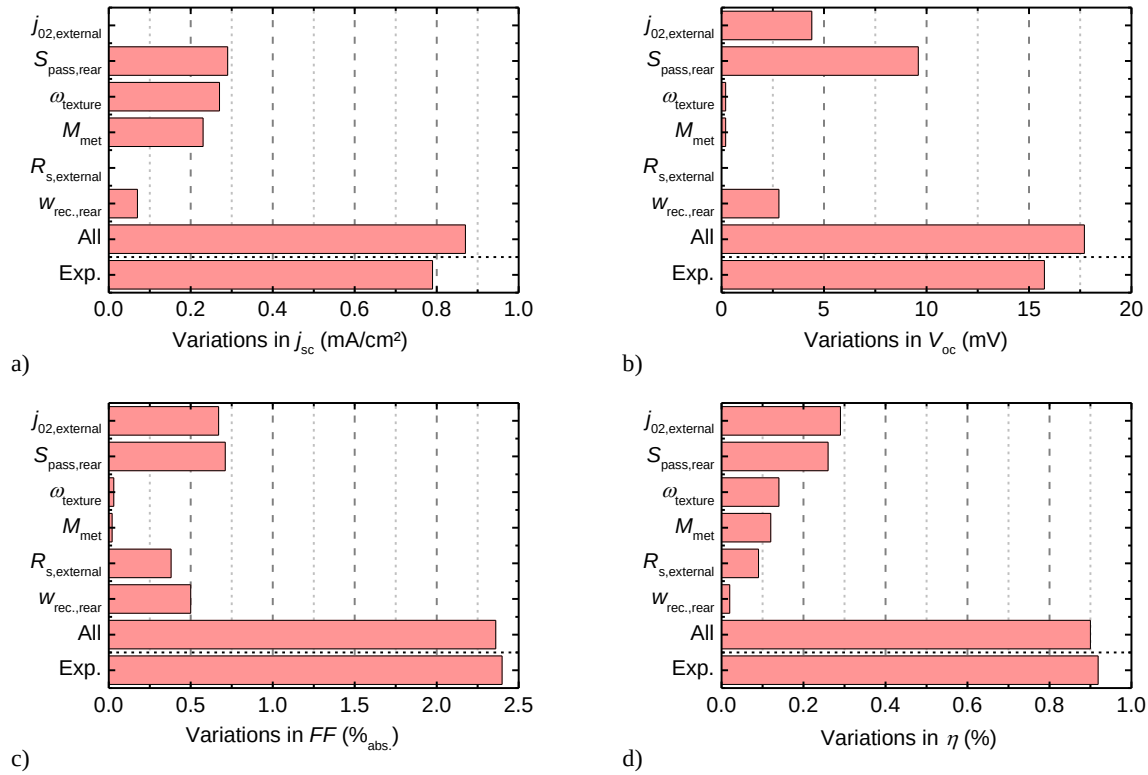

Figure 5: Pareto diagrams of the impact of each input parameter on the total variations in a) short circuit current density j_{sc}, b) open circuit voltage V_{oc}, c) fill factor FF and d) efficiency η ranked by their impact on η. The bottom bar shows the experimental variation that is defined as the difference between the max. and the 10th percentile.

4 DISCUSSION

The measured and simulated distributions are in quite good agreement. The only obvious deviation from the experiment is found to be in the absolute value of the short-circuit current density j_{sc} (Figure 4 a), which could be caused by assuming a wrong level of the shading fraction M_{met} or the SRH parameter τ_{n0}. Nonetheless, the width of the simulated j_{sc} distribution is very similar to the measured one. Most of the outliers in the experiment were caused by severe series and parallel resistance issues and are excluded by choosing the 10th percentile of the measured solar cell characteristic as the minimal value.

Note that our approach of considering only three values (low, med. and high) of each input parameter was not supposed to reflect the shape of the distribution but rather to reproduce the width of the measured distribution. This goal was achieved since for every cell characteristic the min. and max. values of the simulation roughly correspond to the 10th and 100th (= max. value) percentile of the experimental value as shown in Figure 5, including 90 % of the fabricated cells. Since we match the measured variations very well, the neglecting of parameters such as the recombination under the front metallization $S_{met,front}$, variations of the specific contact resistance $\rho_{contact}$ or lateral fluctuations of sizes such as the wafer thickness d_{Si} and the thickness of the ARC layer d_{ARC} are justified. However, they can become relevant when achieved absolute efficiencies are higher and/or total variations are lower.

With the data given in Figure 5 we can clearly prove our thesis (equation (5)) that the sum of all variations caused by each input parameter matches the absolute variation of each of the four cell characteristics.

We account the huge j_{02} influence (on V_{oc} and *FF*) to a wrap-around of liquid during the emitter etch back process. Subsequent finger printing and firing most probably resulted in the formation of recombination active defects in the depletion region between the partially etched emitter and the base. This is underlined by Figure 6, where a dark lock-in thermography image taken at +0.5 V is shown, clearly hinting at power losses at the bottom and right cell edge. A grayscale image of the wafer front side after the emitter etch back process taken under diffuse illumination shows the results of the wrap-around at these edges.

Regarding the variations in short-circuit current density j_{sc}, it is remarkable that the optics, equally represented by $\omega_{texture}$ and M_{met}, only account for less than 60 % of the total variation, recombination at the rear side making up the other big part.

Noteworthy, we find the fill factor *FF* mainly to be influenced by recombinational influences ($j_{02,external}$, $S_{pass,rear}$ and $w_{rec,rear}$), whereby one must mention that in our assumed model for the rear side contacts, the contacted and the damaged area of the LFC contacts increase with increasing $w_{rec,rear}$. Therefore, $w_{rec,rear}$ also has an influence on the contribution of the rear side to the total series resistance. The series resistance contribution of the front side $R_{s,external}$ plays only a minor role in *FF* variations.

The open-circuit voltage V_{oc} is expectedly mostly sensitive to recombination at the rear side. Notably, our absolute values and variations of $j_{02,external}$ or non-ideal recombination respectively, are sufficiently high in order to affect V_{oc}.

The combined impact of $S_{pass,rear}$ on η is smaller than one might expect by summing up the influences on j_{sc}, V_{oc} and *FF*. This can be explained by the fact that the dependence of V_{oc} and j_{sc} on $S_{pass,rear}$ is negative whereas *FF* shows a positive correlation.

Summing it up, the two processes of emitter etch back and rear surface passivation need to be controlled better, since they are responsible for almost 60 % of process-related variations in solar cell efficiency in our applied solar cell fabrication. With a more stable rear surface passivation and avoided wrap-around in the emitter etch back process, the next optimizations should be carried out concerning the optical characteristics of the front side of the cell, namely the texturing process and the finger printing step.

Since in our study the variation of input parameters with “low” and “high” values around the median value leads to roughly symmetric output distributions in the simulations, the same findings for reducing the variations in cell efficiency hold true for raising the absolute level of achieved cell efficiencies in the same manner. This implies that, after optimizing the emitter etch-back process and improving the rear surface passivation, the optics of the front side should be improved.

Tools and methods for the inline characterization of the rear surface passivation on cell precursors or finished cells are not readily available. Hence, special lifetime samples need to be prepared, as in the present work. Future R&D efforts should focus on the development of such methods and stable passivation techniques. For the detection of wrap-around during emitter etch-back, grayscale images taken in the visual spectral range after etch-back and dark lock-in thermography images of finished cells at moderate forward bias are suitable. For controlling the optics of the front surface, reflectance measurements after texturing and visual inspection after metallization can be applied.

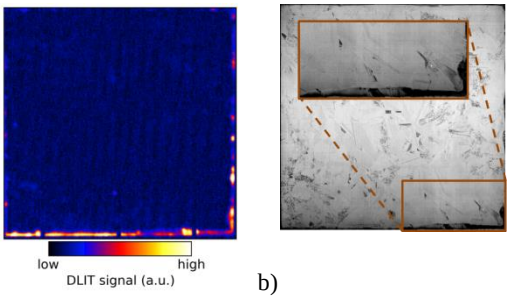

a) b)

Figure 6: a) Dark lock-in thermography (DLIT) image at +0.5 V of a cell with huge pseudo fill factor problems (pFF = 77.7 %, j_{02} = 65 nA/cm², R_p = 5162 Ωcm²). Cleary visible is a power loss at the bottom and right cell edge that is found to be caused by a wrap-around of liquid during the emitter etch back process. Subsequent finger printing and firing most probably resulted in the formation of recombination active defects in the depletion region between the partially etched emitter and the base. b) The grayscale image of the wafer front side after the emitter etch back process taken under diffuse illumination of white light emitting LEDs shows the results of the wrap-around of the etch-process to the front side at these edges.

5 SUMMARY AND CONCLUSION

We introduce a simulation-based approach to investigate the impact of process and parameter variations in a multicrystalline silicon (mc-Si) passivated emitter and rear cell (PERC) process with laser fired contacts (LFC) and verify it with experimental data. An experiment to garner only the process-induced variations and to exclude material-related variations is carried out. The impact of each input parameter is extracted and ranked by its influence on each of the four relevant solar cell performance characteristics, allowing us to spot the crucial processes and parameters that lead to most variations and reductions in efficiency.

In our case we identify the rear side passivation and a wrap-around during the emitter etch back process being in charge of almost 60 % of the process-related fluctuations in efficiency η amounting to $\Delta\eta = 0.9\ \%_{abs.}$. The need to increase the stability of the surface passivation and a suitable inline characterization tool is highlighted.

The presented approach can as well be used for finding ways to improve the absolute level of efficiencies and can be basically transferred to other production lines including e.g. PERC and Al-BSF solar cell manufacturing where it is especially helpful for ramping-up production.

6 ACKNOWLEDGMENT

The experiments of this work were conducted under the frame of the project “Q-Wafer” (03SF0409A and B), supported by the German Ministry for Education and Research (BMBF).

The authors would like to thank the whole team of PV-TEC that helped processing and characterizing and made this work possible.

Nico Wöhrle is appreciatively acknowledged for providing the LFC template for Sentaurus Device.

Sven Wasmer gratefully acknowledges the support by scholarship funds from the State Graduate Funding Program of Baden-Württemberg.

7 REFERENCES

[1] A. W. Blakers, A. Wang, A. M. Milne, J. Zhao, and M. A. Green, “22.8% efficient silicon solar cell,” *Applied Physics Letters*, vol. 55, no. 13, pp. 1363–1365, 1989.

[2] J. Greulich, H. Höffler, U. Würfel, and S. Rein, “Numerical power balance and free energy loss analysis for solar cells including optical, thermodynamic, and electrical aspects,” *J. Appl. Phys*, vol. 114, no. 20, p. 204504, 2013.

[3] M. Müller, P. P. Altermatt, H. Wagner, and G. Fischer, “Sensitivity analysis of industrial multicrystalline PERC silicon solar cells by means of 3-D device simulation and metamodeling,” *IEEE Journal of Photovoltaics*, vol. 4, no. 1, pp. 107–113, 2014.

[4] Synopsis, *Sentaurus TCAD*, 2013.

[5] D. Biro, R. Preu, S. W. Glunz, S. Rein, J. Rentsch, G. Emanuel, I. Brucker, T. Faasch, C. Faller, G. Willeke, and J. Luther, “PV-Tec: Photovoltaic technology evaluation center - design and implementation of a production research unit,” in 2006, pp. 621–624.

[6] S. Werner, E. Lohmüller, S. Maier, A. Kimmerle, A. Spribille, S. Wasmer, F. Clement, and A. Wolf, “Process optimization for the front side of p-type silicon solar cells,” in *29th EUPVSEC Amsterdam: 2014*, 2014, pp. 1342–1347.

[7] E. Schneiderlöchner, R. Preu, R. Lüdemann, S. W. Glunz, and G. Willeke, “Laser-fired contacts (LFC),” in *Wittmann*, Glunz Schultz: WIP-Munich and ETA-Florence, 2001, pp. 1303–1306.

[8] L. K. Mak, C. M. Rogers, and D. C. Northrop, “Specific contact resistance measurements on semiconductors,” *J. Phys. E: Sci. Instrum*, vol. 22, no. 5, pp. 317–321, 1989.

[9] H. Höffler, H. Al-Mohtaseb, J. Haunschild, B. Michl, and M. Kasemann, “Voltage calibration of luminescence images of silicon solar cells,” *J. Appl. Phys*, vol. 115, no. 3, p. 34508, 2014.

[10] R. A. Sinton, A. Cuevas, and M. Stuckings, “Quasi-steady-state photoconductance, a new method for solar cell material and device characterization,” in *Wittmann*, Glunz Rein Isenberg Riepe: IEEE; New York, NY, USA, 1996, pp. 457–460.

[11] J. A. Giesecke, B. Michl, F. Schindler, M. C. Schubert, and W. Warta, “Minority carrier lifetime of silicon solar cells from quasi-steady-state photoluminescence,” *Solar Energy Materials & Solar Cells*, vol. 95, no. 7, pp. 1979–1982, 2011.

[12] B. Michl, M. Rüdiger, J. A. Giesecke, M. Hermle, W. Warta, and M. C. Schubert, “Efficiency limiting bulk recombination in multicrystalline silicon solar cells,” *Sol. Energy Mater. Sol. Cells*, vol. 98, pp. 441–447, 2012.

[13] D. E. Kane and R. M. Swanson, “Measurement of the emitter saturation current by a contactless photoconductivity decay method (silicon solar cells),” in Glunz, 1985, pp. 578–583.

[14] B. T. Phong, “Illumination for computer generated pictures,” *Commun. ACM*, vol. 18, no. 6, pp. 311–317, 1975.

[15] M. A. Green, “Self-consistent optical parameters of intrinsic silicon at 300K including temperature coefficients,” *Sol. Energy Mater. Sol. Cells*, vol. 92, no. 11, pp. 1305–1310, 2008.

[16] S. C. Baker-Finch, K. R. McIntosh, and M. L. Terry, “Isotextured Silicon Solar Cell Analysis and Modeling 1: Optics,” *Photovoltaics, IEEE Journal of*, vol. 2, no. 4, pp. 457–464, 2012.

[17] J. Greulich, A.-K. Volk, N. Wöhrle, I. Haedrich, M. Wiese, M. Hermle, and S. Rein, “Optical Simulation and Analysis of Iso-textured Silicon Solar Cells and Modules Including Light Trapping,” *5th International Conference on Silicon Photovoltaics, SiliconPV 2015*, vol. 77, pp. 69–74, http://www.sciencedirect.com/science/article/pii/S1876610215007791, 2015.

[18] M. Rüdiger and M. Hermle, “Numerical analysis of locally contacted rear surface passivated silicon solar cells,” *Japanese Journal of Applied Physics*, vol. 51, pp. 10NA07, 2012.

[19] A. Fell, K. R. McIntosh, P. P. Altermatt, Janssen, G. J. M, R. Stangl, A. Ho-Baillie, H.

Steinkemper, J. Greulich, M. Müller, B. Min, K. C. Fong, M. Hermle, I. G. Romijn, and M. D. Abbott, "Input parameters for the simulation of silicon solar cells in 2014," *IEEE Journal of Photovoltaics*, vol. 5, no. 4, pp. 1250–1263, 2015.

[20] P. Altermatt, "Models for numerical device simulations of crystalline silicon solar cells—a review," (English), *J Comput Electron*, vol. 10, no. 3, pp. 314–330, 2011.

[21] C. Schwab, "Herstellung und Charakterisierung industrieller oberflächenpassivierter p-typ Solarzellen," Dissertation, Fraunhofer Institut für Solare Energiesysteme ISE, Albert-Ludwigs-University, Freiburg, 2013.

[22] N. Wöhrle, J. Greulich, M. Graf, M. Hermle, and S. Rein, "Efficiency potential simulation for an industrially feasible LFC-PERC concept with sensitivity analysis on crucial cell parameters," in *29th EUPVSEC Amsterdam: 2014*, 2014, pp. 421–426.

[23] A. Schenk and U. Krumbein, "Coupled defect-level recombination: Theory and application to anomalous diode characteristics," *J. Appl. Phys*, vol. 78, no. 5, pp. 3185–3192, 1995.